International Journal of Mathematics and Statistics

ISSN (Online): 2208-2212
Volume 11 Issue 02 June 2025

DOI: https://doi.org/10.53555/n3h59b60

CASSON HYBRID NANOFLUID FLOW AND HEAT TRANSFER PAST AN INFINITE EXPONENTIALLY ACCELERATED VERTICAL POROUS SURFACE WITH CHEMICAL REACTIONS

N.Srinivasa Rao[1*]

[1]Associate Professor, Department of Mathematics, GFGC, kolar, Karnataka, India E-mail : n.s.s.rao2526@gmail.com*

***Abstract**: Casson hybrid nanofluidover an exponentially accelerated vertical porous surface has been considered. Under the influence of slip velocity in a rotating frame, it takes Hall and ion slip impacts into account. Water and ethylene glycol mixture is considered a base Casson fluid. A steady uniform magnetic field is applied under the postulation of a low magnetic Reynolds number. The ramped temperature and time-altering concentration at the surface are considered. First-order consistent chemical reaction and heat absorption are also regarded. Rotating disks involving chemical reactions find extensive applications in the medical field, particularly in optimizing chemical processes for controlled drug delivery systems, thereby improving precision in therapeutic treatments. In this study, we elucidate the behavior of fluid flow over a rotating disk with Casson ternary hybrid nanofluid with incorporation of chemical reactions. Thus, a similarity transformation approach was employed, converting the boundary layer equations into similarity equations represented as ordinary differential equations. Subsequently, the bvp4c solver in MATLAB is utilized to numerically solve the set of non-linear ordinary differential equations describing the boundary value problem. The graphical representations scrutinize the effects of physical parameters on the significant flow characteristics. The expression for non-dimensional shear stress, heat transfer rate and mass transfer are also evaluated. They are tabulated with different variations in implanted parameters.*

***Key words :** Casson Nano fluid, Radial stretching, Numerical simulation, Chemical reaction, Drug delivery.*

1.**Introduction**.

The recent developments in technology require an innovative revolution in heat transfer. The research on nanofluids has been amplified fast. According to reports nanofluids are advantageous heat transport fluids for engineering and manufacturing applications. The heat transport development of nanofluids is principally reliant on the heat conductivity of nanoparticles, particles' volume concentration and mass flow discharges. Under steady particles' volume concentration and flow discharges, the heat transport development only on the heat conductivity of the nanoparticles. The heat conductivity of nanoparticles may be revised or transformed by developing hybrid nanoparticles. Hybrid nanoparticles are nanoparticles created by two or additional different substantial of nanometer scale. The fluids developed through hybrid nanoparticles of transformed metals interested in the base fluid are recognized as hybrid nanofluids. As shown in Figure 1, with this advancement, researchers started to report several challenges associated with hybrid nanofluids soon after they came into the limelight. A large effective diversity of applications are applied in contemporary science, technology and engineering territory, such as chemical manufacture, automobile, solar collector,nuclear reactor, industrial cooling, solar synthesis, gas sensing, bio-sensing, etc. The heat transfer of effective fluids may be improved using a variety of methods. One of these is to hang nanoparticles (Cu, CuO, Ag, Fe, Au, MgO, MoS2, Al, Al2O3, TiO2, etc.) by dimension among 1 and 100nm to the base fluid (e.g. H2O, C2H6O2 (ethylene glycol), C2nH4n+2On+1 (polyethylene-glycol), glycerine, blood, engine oil, (C6H8O6)n (sodium alginate), . . . etc.).

This to improve the constructive thermal characteristics of nanofluids and circumvent discrepancies in the traditional nanofluids. Realistic implementations of these concepts were first conceded by Choi [1] to enhance the heat conductivity and speed of heat transport.Sundar et al. [2] discussed that hybrid nanofluids are additional effectual heat transport fluids than solitary nanoparticle-based nanofluids or traditional fluids. Sarkar et al. [3] opined that appropriate hybridizations may create hybrid nanofluids extremely promising for heat transport development; nevertheless, more investigative works are required in development and immovability, characterizations and applications to defeat the disputes or challenges. Devi et al. [4] explored the magnetohydrodynamic (MHD) flow of Cu-Al2O3/water hybrid nanofluids. Oxide nanoparticles have a lesser amount of heat conductivity than metallic nanoparticles. A superior volume fraction of oxide nanoparticles are required to have the needed heat effectiveness. The computational outcomes indicate that heat replaced the speed of Cupper-alumina/water hybrid nanofluids is more significant than that of the Cu–H2O nanofluids. The characteristics of hybrid nanofluids, based on different kinds of metallic and oxides, such as MgO, Fe3O4, Silver, copper oxide, Copper, and MWCNTs, have been demonstrated by Minea [5]. This showed most excellent viscosity amplification for CuO-Cu hybrid nanoparticles. Toghraie et al. [6] illustrated a variety of correlations for heat conductivities of nanofluids cleared by preceding researchers. They recommended an innovative correlation for the heat conductivity of ZnO-Titania/Ethylene Glycol hybrid nanofluids by highest accurateness using investigational findings. Hayat et al.[7] explored the three-dimensional Brinkman hybrid nanofluids models to examine theheat transport features of Copper oxide/H2O and Silver–CuO/H2O nanofluids past a linearly stretching surface with heat radiation and homogeneous and heterogeneous reactive lows.Anexhaustive and narrative review on heat transport investigation of predictable and hybrid nanofluids by the non-Newtonian fluid model was determined by Jamshed et al.[8] and Ellahi [9]. Aman et al. [10] exhibited the sodium alginate-based hybrid nanofluids (Copper-Alumina) flow in vertical ducts. Usman et al. [11] discussed the nonlinear thermal radiation and time-dependent heat conductivity due to rotating flow alumina-H2O hybrid nanofluids past a stretching sheet with a magnetic field and buoyancy force. Despite the complications of producing non-Newtonian fluids, applied mathematicians and engineers are engaged in non-Newtonian fluid mechanics. Because the flow and heat transport features of those fluids are significant to numerous and miscellaneous systems in bio-technology, pharmaceutical and chemical engineering, etc. Non-Newtonian modelling has a nonlinear relationship with the stress and rate of strain. The mechanical features of non-Newtonian fluids, and hear thin or shear thickness, usual stress difference, and visco-elastic reaction, may not be portrayed through the conservative theories; hence, an innovative and effectual prediction is required. Various constitutive equations portray the movement and heat transport mechanism, along with these; the Casson model has grown a great deal of acceptance. Casson fluid model becomes a non-Newtonian fluid to the investigators due to its wide-range applications in biomedical and industrial engineering, energy production, geophysical fluid mechanics and dynamics. Among plentiful non-Newtonian models, Casson fluid model is the mainly significant rheological model, established by Casson [12]. Casson fluid is a shearing thin fluid processed as one type of non-Newtonian fluid.

This exhibited yield stresses. If a lesser amount of shear stress than the yield stress is applied, then the fluid performs like a solid that is, there is no flow and it moves if the applying shear stress is superior to the yield stress (Ghosh and Mukhopadhyay [13]). In this shearing thin fluid model, it is assumed to have an unlimited viscosity near the vanish rate of shear, yield stress below this no flow take places and a zero viscosity near an infinite rate of shear stress. Tomato sauce, Jellies, honey, human blood, soup, biological fluids, etc. are a number of frequent samples of Casson fluids. The virtual investigation of Casson fluid through homogeneous and heterogeneous reactions was examined by Khan et al. [14].Nayak et al. [15] explored the three-dimensional unsteady MHD flow and the entropy generation of micropolar Casson cross nanofluid with nonlinear thermal radiation, chemical reaction, Brownian motion, thermophoresis effect, convective boundary conditions, viscous dissipation and Joule heating. Rasoola et al. [16] discussed the features of Casson kind nanofluid flow through a porous medium past a nonlinear stretching surface with heat and mass transport improvements. A numerical study of Casson nanofluid over parallel stretching plane with magnetic field and Joule heating with slip and heat convective boundary conditions was presented by Kamran et al. [17].

Nanofluids allow for better control over the dispersion of nanoparticles in chemical reaction mediums which results in more uniform reaction conditions, ensuring consistent product quality in the industrial processes. Despite the unique

properties and potential applications of hybrid nanofluids, there are still challenges to overcome, such as the increase in viscosity, which leads to higher pumping power requirements, and the stability of hybrid suspension particles [18]. Thus, a vast body of research has been devoted to study the impact of nanofluids in fluid flow with respect to chemical processes and its practical applications in the growing engineering industry. As discussed in the work of [19] chemical reactions in fluid systems are generally divided into two categories: homogeneous reactions, which occur uniformly throughout the fluid medium, and heterogeneous reactions, which take place on distinct catalytic surfaces as. In reactive flow systems, particularly those involving nanofluids or bloodbased fluids over a rotating disk, both homogeneous and heterogeneous reactions play vital roles in determining concentration and mass transfer characteristics. Homogeneous reactions occur within the fluid bulk, representing volumetric chemical transformations such as enzymatic or drug reactions within the bloodstream. In contrast, heterogeneous reactions take place at the boundary surface typically at the rotating disk mimicking surface interactions such as drug-tissue binding or catalytic activity on biomedical implants. The coupling of these reactions under the influence of rotation, shear forces, and thermal gradients leads to complex transport behavior. Modeling both types of reactions simultaneously allows for a more realistic simulation of biomedical processes, such as targeted drug delivery, dialysis, or nanoparticleassisted therapy, where reaction kinetics at both the fluid and surface levels are significant. These reactions serve critical roles in a variety of chemical systems, including catalysis, biological processes, and combustion. Chaudhary and Merkin [19] were pioneers in investigating the boundary layer flow concerning homogeneous and heterogeneous chemical reactions. Their study marked the initial exploration of this aspect in the context of chemical reactions occurring within the boundary layer. Thereupon Merkin [20] expanded on their revolutionary findings by studying chemical reactions in fluid dynamics, utilizing cubic autocatalysis principles and including a first-order mechanism for heterogeneous reactions. The purpose of this experiment was to better comprehend viscous liquid flow across a stretched surface. The theoretical advancements in von-Kármán boundary layer flow have rapidly evolved, adapting to various contexts that align closely with chemical reaction with strong industrial demands. For instance, He et al. [21] experimented heat transmission characteristics of power law fluid over porous spinning disk, Gangadhar et al. [22] elucidated the MHD flow of an current carrying Maxwell fluid across a radially stretching or shrinking spinning disc with chemical reactions. Recently, Alharbi et al. [23] probed the impact of surface-catalyzed reactions on the flow of a rotating disk covered by a temperaturedependent viscosity fluid. The results demonstrate consistent reduction for both mass diffusion rate and wall concentration as the parameters of porosity and surface catalysis undergo variations. A significant body of research has been conducted to explore the intricacies of fluid dynamics on stretching/shrinking surfaces, with a particular emphasis on the Casson fluid with comprehensive analysis of both homogeneous and heterogeneous reactions, unraveling the complexities inherent in fluid phenomena. Sheikh and Abbas [24], Mustafa et al. [25], Bhattacharyya [26] and Mukhopadhyay et al. [27] explored the impact of homogeneous-heterogeneous reactions on the boundary layer flow of Casson fluid, near a stagnation point over a porous stretching/shrinking sheet subjected to constant suction. The studies highlight the possibility of a unique solution for all values of the stretching parameter while solutions for the shrinking parameter are constrained to limited ranges. The thermophoresis and Brownian motion phenomena in Casson nanofluid flow over a stretching surface with convective boundary conditions have been investigated by Deebani et al. [28]. The results revealed that increasing the stretching and Casson parameters led to a reduction in the temperature profile. Furthermore, the investigation of dual solutions in Casson fluid flow over moving surfaces has been extensively undertaken by Hamid et al. [29], Kumar et al. [30], Khan et al. [31], Haldar et al. [32], Mousavi et al. [33] and Fadhel et al. [34] providing valuable insights into the complexities of fluid flow followed by stability analysis. These studies revealed that the existence of multiple solutions is intricately dependent on the dual nature of the stretching or shrinking parameter. With heightened velocity profiles for the Casson fluid over the surface in the upper branch solution, while decreasing velocity patterns define the lower branch solution. Stability analysis unveils that the first solution is stable, whereas the second solution is considered unstable. In the domain of the rotating disk configuration, Sahoo and Nandkeolyar [35], Ragupathi et al. [36], Ahmed et al. [37], Ramzan et al.[38] have shed light on key outcomes that focus on Casson fluid flow with chemical processes. The study's conclusion highlights pronounced effectiveness of homogeneous and heterogeneous chemical reaction parameters in diminishing concentration distribution and alter the fluid's properties, such as viscosity and thermal conductivity affecting the velocity and temperature profiles. These papers collectively demonstrate that the behavior of Casson nanofluids in rotating disk systems is highly sensitive to autocatalytic, thermal, and rotational effects. These insights are essential for advanced thermal management and bioengineering applications Evidently, homogeneous and heterogeneous reactions occurring in the fluid flow over rotating disks have the potential to enhance system entropy optimization, thereby contributing to increased efficiency and lowered energy consumption in diverse industrial processes. A critical examination of the existing literature reveals a significant gap in research focus, particularly regarding the Casson nanofluid over rotating disk geometries. This study addresses this notable void by aiming to comprehensively analyze the flow patterns within the context of the Casson fluid, incorporating chemical reactions and mass transfer characteristics, and considering both homogeneous and heterogeneous reactions. Therefore, this study aims at revealing novel results on the heat and mass transfer of Casson ternary hybrid nanofluid over stretching rotating disk subjected to chemical reactions which has not been investigated thus far in other studies. The study utilizes similarity transformations applied to the governing set of nonlinear partial differential equations, which include mass, momentum, and concentration equations. These transformations convert the equations into ordinary differential equations and subsequently, the bvp4c function within the MATLAB software is employed to numerically solve the simplified set of ordinary differential equations.

2.Formulation of the problem.

The physical model of the present study is displayed in Figure.1 The x-axis is taken along the surface in the vertically growing path, the z-axis is perpendicular to the surface and the y-direction is at right angles to the xz-plane. The plate and fluid have been considered in a situation of an inflexible body rotating through a uniform angular velocity Ω on the z-direction. Initially, at the time $t = 0$, the surface and the adjoining fluid are at respite to an invariable free stream temperature T_∞ and concentrations far left from the surface C_∞. At the time $t > 0$, the plate starts accelerating proportionally by the side of the x-axis associated with the gravitation field with a velocity $u_0 e^{t/t_0}$, where u_0 is a constant and t_0 is the characteristic time. The surface temperature is brought up or depressed to $T_\infty + (T_w - T_\infty)(t/t_0)$ if $0 < t \leq t_0$ and afterward this is continued at uniform temperature

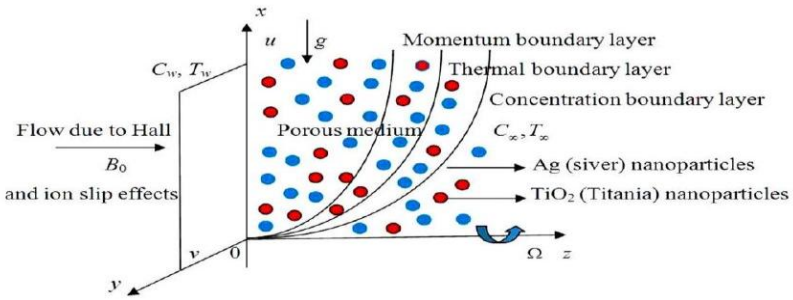

Fig.1.Physical configuration of the problem

The fundamental rheological equations of Cauchy stress tensor for an isotropic and an incompressible fluid flow of a Casson model may be shown in the following form

$$\tau = \left(\mu_b + \frac{p_y}{\sqrt{2\pi}}\right) 2e_{ij}, \quad \pi > \pi_c; \left(\mu_b + \frac{p_y}{\sqrt{2\pi_c}}\right) 2e_{ij}, \quad \pi < \pi_c \tag{1}$$

where π is the product of the component of deformation rate through itself, namely, $\pi = e_{ij}e_{ij}, e_{ij}$ is the $(i,j)^{\text{th}}$ component of the rate of deformation and π_c is the significant estimation of π based on the non-Newtonian model. If $\pi < \pi_c$, the fundamental rheological equations of Casson fluid reduce as

$$\tau_{ij} = \mu_b \left(1 + \frac{1}{\beta}\right) 2e_{ij} \tag{2}$$

where $\beta = \mu_b \frac{\sqrt{2\pi}}{p_y}$. When $\beta \to \infty$, the non-Newtonian behavior of the fluid disappears, and the fluid performs similarly to a Newtonian fluid. Under the exceeding referred assumptions, and assuming Boussinesq approximation for body force term, the momentum equation governing the unsteady MHD flow of Cassonnanofluids by permeable media in a rotating frame are as

$$\begin{aligned} \rho_{hnf}\left(\frac{\partial q}{\partial t} + (q.\nabla)q + 2\Omega \times q\right) =& -\nabla p + \mu_{hnf}\left(1 + \frac{1}{\beta}\right)\nabla^2 q + (J \times B) \\ & - \frac{\mu_{hnf}}{K^*}\left(1 + \frac{1}{\beta}\right) q + g(\rho\beta_T)_{hnf}(T - T_\infty) \\ & + g(\rho\beta_C)_{hnf}(C - C_\infty) \end{aligned} \tag{3}$$

The component forms of Equation (3) when the pressure term is neglected

$$\begin{aligned} \frac{\partial u}{\partial t} - 2\Omega v =& v_{hnf}\left(1 + \frac{1}{\beta}\right)\frac{\partial^2 u}{\partial z^2} + \frac{B_0 J_y}{\rho_{hnf}} - \frac{v_{hnf}}{K^*}\left(1 + \frac{1}{\beta}\right) u \\ & + g(\beta_T)_{hnf}(T - T_\infty) + g(\beta_C)_{hnf}(C - C_\infty) \\ \frac{\partial v}{\partial t} + 2\Omega u =& v_{hnf}\left(1 + \frac{1}{\beta}\right)\frac{\partial^2 v}{\partial z^2} - \frac{B_0 J_X}{\rho_{hnf}} - \frac{v_{hnf}}{K^*}\left(1 + \frac{1}{\beta}\right) v \end{aligned} \tag{4}$$

The electron and atom collisions are assumed to be highly elevated; consequently, the Hall and ion slip impacts may not be deserted. For this reason, the Hall and ion slip consequences increase to the velocity in the y-direction.

$$J = \sigma(E + V \times B) - \frac{\omega_e \tau_e}{B_0}(J \times B) + \frac{\omega_e \tau_e \beta_i}{B_0^2}((J \times B) \times B)\Big) \tag{5}$$

Additionally, it is assumed that $\omega_e \tau_e \sim O(1)$and $\omega_i \tau_i << 1$, in Equation (5), the electron pressure gradient and thermo-electric effects are abandoned, i.e. the electric field $E = 0$ under these assumptions, Equation (5) is condensed to be

$$\begin{aligned}(1 + \beta_i \beta_e) J_x + \beta_e J_y &= \sigma B_0 V \\ (1 + \beta_i \beta_e) J_y - \beta_e J_x &= -\sigma B_0 u\end{aligned} \tag{6}$$

On solving Equation (6) we obtain

$$\begin{aligned}J_x &= \sigma B_0(\alpha_2 u + \alpha_1 v) \\ J_y &= -\sigma B_0(\alpha_2 v - \alpha_1 u)\end{aligned} \tag{7}$$

where$\alpha_1 = \frac{1+\beta_e\beta_i}{(1+\beta_e\beta_i)^2+\beta_e^2}$ and $\alpha_2 = \frac{\beta_e}{(1+\beta_e\beta_i)^2+\beta_e^2}$ Substituting Equation (6) in (4) accordingly, the equation of continuity, the momentum equation, energy and concentration equations are acquired.

$$\begin{aligned}\frac{\partial u}{\partial x} + \frac{\partial v}{\partial y} &= 0 \\ \frac{\partial u}{\partial t} - 2\Omega v &= v_{hnf}\left(1 + \frac{1}{\beta}\right)\frac{\partial^2 u}{\partial z^2} + \frac{\sigma_{hnf} B_0^2(\alpha_2 v - \alpha_1 u)}{\rho_{hnf}} - \frac{v_{hnf}}{K^*}\left(1 + \frac{1}{\beta}\right)u \\ &\quad + g(\beta_T)_{hnf}(T - T_\infty) + g(\beta_C)_{hnf}(C - C_\infty) \\ \frac{\partial v}{\partial t} + 2\Omega u &= v_{hnf}\left(1 + \frac{1}{\beta}\right)\frac{\partial^2 v}{\partial z^2} - \frac{\sigma_{hnf} B_0^2(\alpha_2 u + \alpha_1 v)}{\rho_{hnf}} - \frac{v_{hnf}}{K^*}\left(1 + \frac{1}{\beta}\right)v \\ (\rho C_p)_{hnf}\frac{\partial T}{\partial t} &= k_{hnf}\frac{\partial^2 T}{\partial z^2} - Q_0(T - T_\infty) \\ \frac{\partial C}{\partial t} &= D_{hnf}\frac{\partial^2 C}{\partial z^2} - Kr^*(C - C_\infty)\end{aligned} \tag{8}$$

The initial and boundary conditions for the flow past the electrically non-conducting plate with slip velocity are

$$\begin{aligned}&u = v = 0, T = T_\infty, C = C_\infty, \quad t \le 0, z > 0 \\ &u = u_0 e^{t/t_0} + \lambda_0\left(1 + \frac{1}{\beta}\right)\frac{\partial u}{\partial z}, v = \lambda_0\left(1 + \frac{1}{\beta}\right)\frac{\partial v}{\partial z} \\ &T = \begin{cases} T_\infty + (T_w - T_\infty)(t/t_0), & \text{if } 0 < t \le t_0 \\ T_w & \text{if } t > t_0 \end{cases} \\ &C = C_\infty + (C_w - C_\infty)(t/t_0) \\ &u \to 0, v \to 0, T \to T_\infty, C \to C_\infty, t > 0, \text{ as } z \to \infty\end{aligned} \tag{9}$$

The characteristic time t_0 may be defined in accordance with the non-dimensional procedure as $t_0 = v_{hnf}/u_0^2$.

$$\begin{aligned}\rho_{hnf} &= (1 - \phi_2)\left[(1 - \phi_1)_{\rho f} + \phi_1 \rho_{s_1}\right] + \phi_2 \rho_{s_2}, \mu_{hnf} = \frac{\mu_f}{(1 - \phi_1)^{2.5}(1 - \phi_2)^{2.5}}, \\ \sigma_{hnf} &= \sigma_{bf}\left[\sigma_{s_2}(1 + 2\phi_2) + 2\sigma_{bf}(1 - \phi_2)\sigma_{s_2}(1 - \phi_2) + \sigma_{bf}(2 + \phi_2)\right], \\ \sigma_{bf} &= \sigma_f\left[\sigma_{s_1}(1 + 2\phi_1) + 2\sigma_f(1 - \phi_1)\sigma_{s_1}(1 - \phi_1) + \sigma_f(2 + \phi_1)\right], \\ (\rho\beta_T)_{hnf} &= (1 - \phi_2)\left[(1 - \phi_1)(\rho\beta_T)_f + \phi_1(\rho\beta_T)_{s_1}\right] + \phi_2(\rho\beta_T)_{s_2}, \\ (\rho\beta_C)_{hnf} &= (1 - \phi_2)\left[(1 - \phi_1)(\rho\beta_C)_f + \phi_1(\rho\beta_C)_{s_1}\right] + \phi_2(\rho\beta_C)_{s_2}, \\ (\rho C_p)_{hnf} &= (1 - \phi_2)\left[(1 - \phi_1)(\rho C_p)_f + \phi_1(\rho C_p)_{s_1}\right] + \phi_2(\rho C_p)_{s_2}, \\ k_{hnf} &= k_{bf}\left[\frac{k_{s_2} + 2k_{bf} - 2\phi_2(k_{bf} - k_{s_2})}{k_{s_2} + 2k_{bf} + \phi_2(k_{bf} - k_{s_2})}\right], k_{bf} = k_f\left[\frac{k_{s_1} + 2k_f - 2\phi_1(k_f - k_{s_1})}{k_{s_1} + 2k_f + \phi_1(k_f - k_{s_1})}\right], \\ D_{hnf} &= (1 - \phi_1)(1 - \phi_2)D_f\end{aligned} \tag{10}$$

where $\phi_1 = 0$ (exclusive of suspension of silver nanoparticles) represents titania/ H_2O and ethylene glycol (Casson) nanofluids and $\phi_2 = 0$ (exclusive of suspension of TiO_2 nanoparticles) represents TiO_2/H_2O and ethylene glycol (Casson) nanofluid. Both $\phi_1 = 0 = \phi_2$ correspond to the base fluid (H_2O and ethylene glycol).

Combining Equations let $q = u + iv$, we obtain that

$$\frac{\partial q}{\partial t} + 2i\Omega q = v_{hnf}\left(1+\frac{1}{\beta}\right)\frac{\partial^2 q}{\partial z^2} - \frac{\sigma B_0^2(\alpha_1 + i\alpha_2)}{\rho_{hnf}}q - \frac{v_{hnf}}{K^*}\left(1+\frac{1}{\beta}\right)q + g(\beta_T)_{hnf}(T - T_\infty) + g(\beta_C)_{hnf}(C - C_\infty) \tag{11}$$

The non-dimensional variables are introduced as

$$u* = \frac{u}{u_0}, v* = \frac{v}{u_0}, z* = \frac{z}{\sqrt{v_f t_0}}, t* = \frac{t}{t_0}, \theta = \frac{T - T_\infty}{T_w - T_\infty}, \phi = \frac{C - C_\infty}{C_w - C_\infty}, M^2 = \frac{\sigma_f B_0^2 v_f}{\rho_f u_0^2}$$

Table 1. Thermophysical properties of H_2O and ethylene glycol, Agand TiO_2.

Physical properties	Water	Ethylene glycol	Ag	TiO_2
$\rho(\mathrm{kg/m^3})$	996.1	1108	10500	4258
$C_p(\mathrm{J/kgK})$	4189	2410	242	689.2
$K(\mathrm{W/mK})$	0.634	0.255	430	8.9528
$\beta \times 10^{-5}(1/\mathrm{K})$	20	-	1.98	0.9
$\sigma(\mathrm{S/m})$	5.5×10^{-6}	-	62.1×10^6	2.6×10^6

$$R^2 = \frac{\Omega v_f}{u_0^2}, K = \frac{K^* u_0^2}{v_f^2}, \mathrm{Gr} = \frac{g(\beta_T)_f v_f (T_w - T_\infty)}{u_0^3}, \mathrm{Gc} = \frac{g(\beta_C)_f v_f (C_w - C_\infty)}{u_0^3}$$

$$\mathrm{Pr} = \frac{(\mu C_p)_f}{k_f}, Q = \frac{Q_0 v_f}{(\rho C_p)_f u_0^2}, \mathrm{Sc} = \frac{v_f}{D_f}, \mathrm{Kr} = \frac{\mathrm{Kr}^* v_f}{u_0^2}$$

Using dimensionless variables, the following governing equations are obtained.

$$J_1\frac{\partial q}{\partial t} = J_2\left(1+\frac{1}{\beta}\right)\frac{\partial^2 q}{\partial z^2} - \left(J_3 M^2(\alpha_1 + i\alpha_2) + 2iR^2 + \frac{J_2}{K}\left(1+\frac{1}{\beta}\right)\right)q + J_4 \mathrm{Gr}\theta + J_5 \mathrm{Gc}\phi$$

$$J_6\frac{\partial \theta}{\partial t} = \frac{J_7}{\mathrm{Pr}}\frac{\partial^2 \theta}{\partial z^2} - Q\theta$$

$$\frac{\partial \phi}{\partial t} = \frac{J_8}{\mathrm{Sc}}\frac{\partial^2 \phi}{\partial z^2} - \mathrm{Kr}\phi \tag{12}$$

The relevant non-dimensional initial and boundary conditions are as follows:

$$q = 0, \theta = 0, \phi = 0 \text{ for all } z > 0 \text{ and } t \le 0,$$

$$q = e^t + \lambda\left(1+\frac{1}{\beta}\right)\frac{\partial q}{\partial z}, \theta = \begin{cases} t & \text{if } 0 < \tau \le 1 \\ 1 & \text{if } \tau > 1 \end{cases}, \phi = t \text{ at } z = 0,$$

$$q \to 0, \theta \to 0, \phi \to 0 \text{ as } z \to \infty \text{ for } t > 0 \tag{13}$$

where $\lambda = \frac{\lambda_0 u_0}{v_f}$ is the slip parameter.

To solve the Equations (12) using the Laplace transform technique with respect to the initial and boundary conditions(13) , the transformed equations of (12) become

$$a_1\frac{d^2\bar{q}}{dz^2}-(s+\lambda_1)\bar{q}=-a_2\bar{\theta}-a_3\bar{\phi}$$
$$\frac{d^2\bar{\theta}}{dz^2}-(s+a_5)a_4\bar{\theta}=0$$
$$\frac{d^2\bar{\phi}}{dz^2}-(s+\mathrm{Kr})a_{10}\bar{\phi}=0 \quad (14)$$

The boundary conditions in terms of transformed variables are as

$$\bar{q}=\frac{1}{s-1}+\lambda\left(1+\frac{1}{\beta}\right)\frac{d\bar{q}}{dz},\bar{\theta}=\frac{1}{s^2}(1-e^{-s}),\bar{\phi}=\frac{1}{s^2}\ \text{at}\ z=0$$
$$\bar{q}\to 0,\bar{\theta}\to 0,\bar{\phi}\to 0 \quad \text{as}\ z\to\infty \quad (15)$$

Solving differential Equations (14) with the boundary conditions (15),we acquire the transformed solutions for velocity, temperature and concentrations $\bar{q}(z,s)$, $\bar{\theta}(z,s)$ and $\bar{\phi}(z,s)$ as

$$\bar{q}(z,s)=\left\{\left(1+\lambda b_5\left(1+\frac{1}{\beta}\right)\right)^{-1}\left[\frac{1}{s-1}+b_3+b_4+\lambda\left(1+\frac{1}{\beta}\right)(b_1+b_2)\right]\right\}e^{-b_5 z}$$
$$-b_3e^{-b_1 z}-b_4e^{-b_2 z}$$
$$\bar{\theta}(z,s)=\frac{1}{s^2}(1-e^{-s})e^{-\sqrt{(s+a_5)a_4}z}$$
$$\bar{\phi}(z,s)=\frac{1}{s^2}e^{-\sqrt{(s+\mathrm{Kr})a_{10}}z} \quad (16)$$

Taking the inverse Laplace transforms for Equations (16), we acquire the solutions for the velocity distribution, temperature and concentration distributions after moving on the t-direction for the flow near a vertical surface with the ramped plate temperature specified as

$$q(z,t)=q_1(z,t)-H(t-1)q_1(z,t-1)$$
$$\theta(z,t)=f_1(\alpha_2,a_5,t)-H(t-1)f_1(\alpha_3,a_5,t-1)$$
$$\phi(z,t)=f_1(\alpha_3,\mathrm{Kr},t) \quad (17)$$

To emphasize the consequence of the ramped wall temperature on the flow field, this may be consequential to contrast such a nanofluid flow due to the uniform wall temperature. In the present case, the initial and boundary conditions (16) are identical, excluding the condition $\theta(0,t)=1$, for $t=0$. Under the assumptions portrayed in this present paper, it is revealed that the temperature distribution and velocity fields for the flow over a surface by the uniform wall temperature may be articulated as follows.

$$q(z,t)=q_2(z,t)$$
$$\theta(z,t)=f_7(\alpha_1,a_5,0,t) \quad (18)$$

Equation (18) represent the velocity and temperature distribution for the uniform wall temperature and the time-altering concentration distribution, respectively.

For the ramped wall temperature

$$\tau=\tau_x+i\tau_y=\left(\frac{\partial q}{\partial z}\right)_{z=0}=q_3(t)-H(t-1)q_3(t-1)$$

For the uniform wall temperature

$$\tau=\tau_x+i\tau_y=\left(\frac{\partial q}{\partial z}\right)_{z=0}=q_4(t) \quad (19)$$

3.Nusselt number. The Nusselt number in terms of rate of heat transport near the plate surface $(z=0)$ for the ramped wall temperature and the uniform wall temperature is derived

$$\theta'(0,t)=-\left(\frac{\partial\theta}{\partial z}\right)_{z=0}=-\sqrt{a_4}\left(g_1(a_5,t)-H(t-1)g_1(a_5,t-1)\right)$$
$$\theta'(0,t)=-\left(\frac{\partial\theta}{\partial z}\right)_{z=0}=-\sqrt{a_4}g_7(a_5,0,t) \quad (20)$$

4.Sherwood number. The Sherwood number in terms of rate of mass transport near the plate surface $(z=0)$

$$\phi'(0,t) = -\left(\frac{\partial \phi}{\partial z}\right)_{z=0} = -\sqrt{a_{10}}g_1(\mathrm{Kr},t) \tag{21}$$

5.Discussion of the numerical results.

The MATLAB solver bvp4c enhances the accuracy of predicting the influence of dimensionless numbers in boundary value problems (BVPs) through a combination of adaptive mesh refinement, collocation methods, and error control. Furthermore, The use of the bvp4c scheme offers a significant advantage in terms of accuracy and computational efficiency. Its adaptive mesh refinement and built-in error control enable it to handle nonlinear boundary value problems more robustly than shooting methods, which are sensitive to initial $\zeta \to \infty$

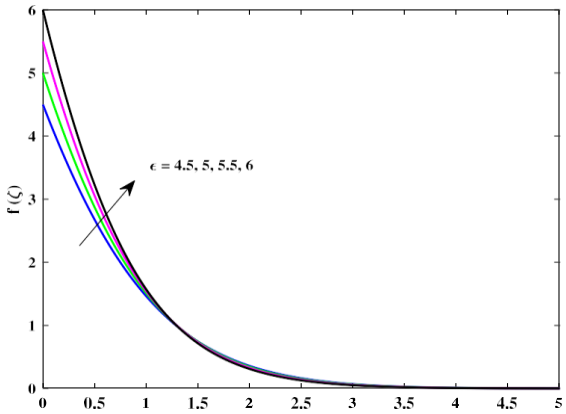

Fig.2 $f(\zeta)$ vs ζ whenβ=0.3,ϑ=3,K=Ks=0.5 and φ1=φ2=φ3=0.05.

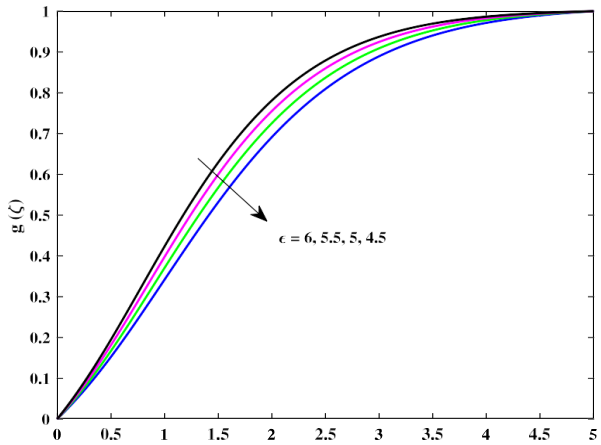

Fig.3 $g(\zeta)$vsζwhenβ=0.3,ϑ=3,K=Ks=0.5andφ1=φ2=φ3=0.05.

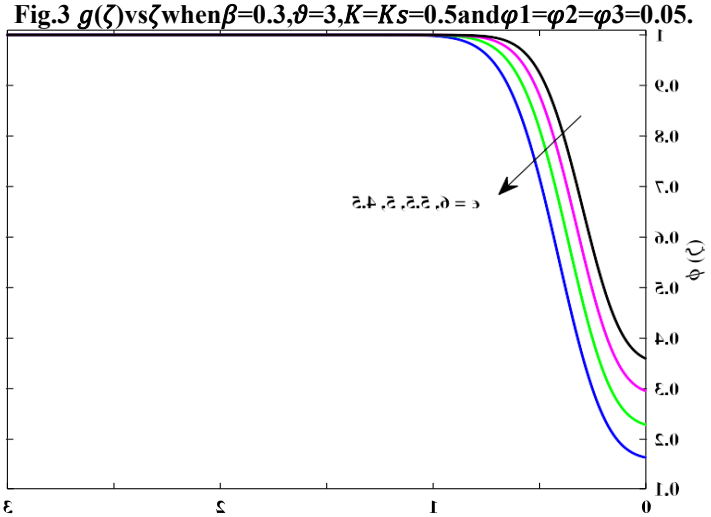

Fig.4.$h(\zeta)$vsζwhenβ=0.3,ϑ=3,K=Ks=0.5andφ1=φ2=φ3=0.05.

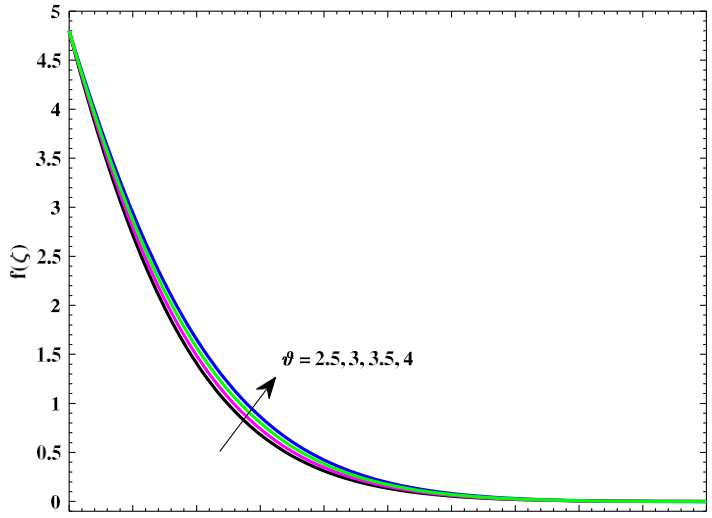

Fig.5. $\phi(\zeta)$vsζwhenβ=0.3,ϑ=3,K=Ks=0.5andφ1=φ2=φ3=0.05.

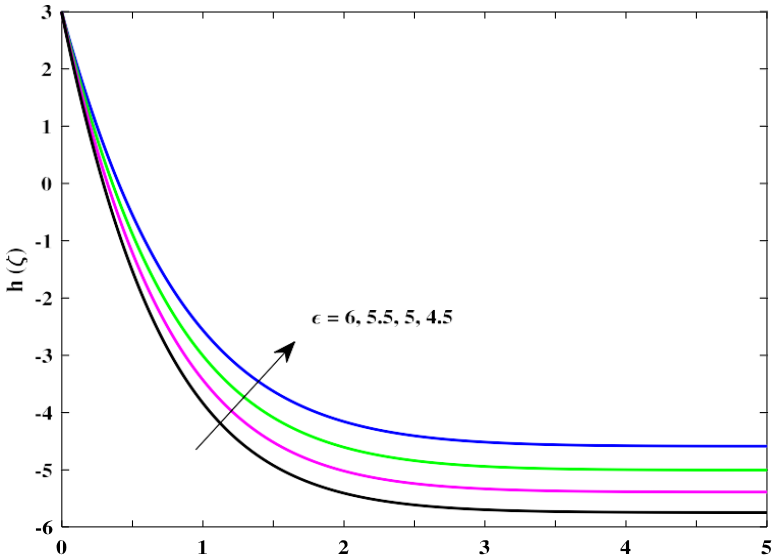

Fig.6. $f(\zeta)$vsζwhenβ=0.3,ϵ=4.8,K=Ks=0.5andφ1=φ2=φ3=0.05.

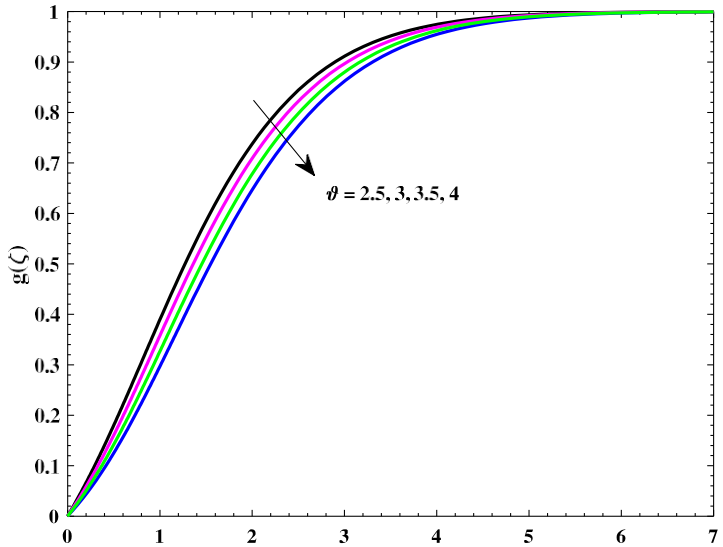

Fig.7. $g(\zeta)$vsζwhenβ=0.3,ϵ=4.8,K=Ks=0.5andφ1=φ2=φ3=0.05.

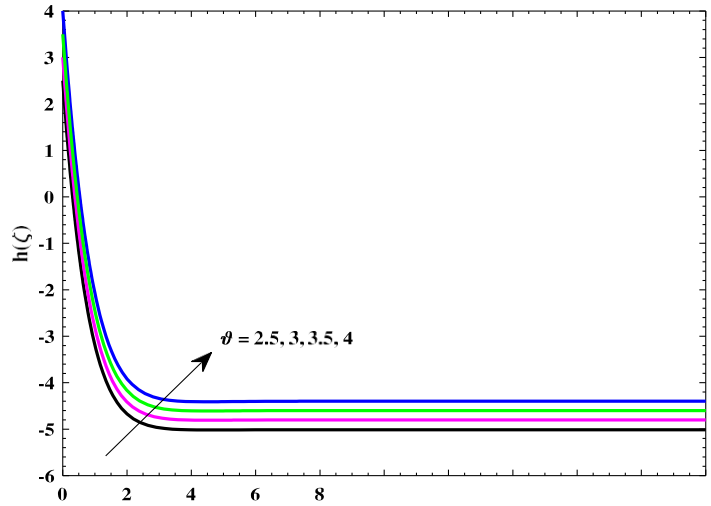

Fig.8. $h(\zeta)$vsζwhenβ=0.3,ϵ=4.8,K=Ks=0.5and$\varphi 1$=$\varphi 2$=$\varphi 3$=0.05.

In Figs. 2–5, the graphs exhibit distinct flow fields represented by f, g, and h, along with the con
centration field ϕ. This comprehensive display thoroughly investigates the response of variations in the disk stretching parameters for the flow and concentration gradients. When the stretching parameter of the rotating disk increases, it implies thatthe radius of the disk increases or its shape becomes more elongated. This stretching effect alters the flow dynamics of the fluid on the disk's surface. An increase in the stretching parameter enhances the radial and tangential velocity component along the disk's surface as shown in Figs. 2 and 3. The enhancement of tangential velocity leads to greater circumferential flow and fluids moves more vigorously around the axis of rotation due to increased centrifugal forces caused by the stretching disk and physically interpreting, more fluid is directed towards the Figs. 6–9 show the distribution of velocity components and concentration profiles for different suction strength values. When the permeability is incorporated into the diffusive region of the disk, the amplitude of the rotation drops considerably. The axial flow becomes stronger as ϑ intensifies because physically more fluid is injected into the surface of the disk and contributes to a stronger axial flow. As the injection parameter increases, the pressure gradient-induced inward radial flow becomes faster due to higher pressure within the system leading to a steeper pressure gradient, which in turn drives a faster inward radial flow where fluid moves from regions of higher pressure at the surface of the disk to lower pressure at the center of the rotating disk. In contrast, as the suction intensifies the circumferential flow denoted by the $g(\zeta)$ profiles tend to decelerate owing to escape of fluid through the disk surfaces. This escape of fluid reduces the fluid's momentum in the circumferential direction, causing a deceleration of the circumferential flow. In essence, as ϑ intensifies, theaxial flow strengthens and the pressure gradient-induced inward radial flow accelerates, while the presence of wall permeability causes the circumferential flow to decelerate due to the loss of fluid through the walls. The results in Fig. 8 reveals that a higher volume of fluid is drawn toward the disk for increasing values of mass flux ϑ.

Table.2 Numerical results of local skin friction, concentration gradient and local
Nusselt number across various governing parameters.

v	e	K=Ks	β	$Re_r^{1/2}cf$	$\Phi^1(0)$	$Re_r^{-1/2}Nu$
2.5	4.8	0.5	0.3	32.92852	0.213948	0.077878
3	-	-	-	31.28795	0.112494	0.020258
3.5	-	-	-	29.73654	0.048274	0.012626
4	-	-	-	25.56761	0.020412	0.012825
-	4.5	-	-	30.13106	0.027669	0.012629
-	5	-	-	35.00804	0.037868	0.012829
-	5.5	-	-	39.89612	0.050477	0.012547
-	6	-	-	40.18548	0.049399	0.012678
-	-	1	-	40.18428	0.044226	0.012481
-	-	2.5	-	40.19524	0.036544	0.059856
-	-	5	-	40.15212	0.025657	0.048258
-	-	10	-	39.67197	0.028251	0.035456
-	-	-	0.2	49.75431	0.024158	0.012456
-	-	-	0.4	34.77868	0.024967	0.012365
-	-	-	0.6	28.78273	0.022189	0.012286
-	-	-	0.8	25.49319	0.021059	0.012311

This is owing to the fact as the Casson fluid parameter increases, the fluid behaves more solid-like, causing the boundary layers to thicken and the overall heat transfer efficiency to decrease, which is reflected in a lower Nusselt number (Table.2).

6.Conclusions: Comprehensive model, especially for high-temperature or microscale applications. Future research can extend this model by including magnetic fields (MHD effects), variable viscosity, and advanced chemical kinetics. Investigating unsteady flow behavior or slip conditions at the boundary can further improve the applicability to microfluidic or biomedical devices. These research directions collectively aim to advance the understanding and practical implementation of Casson fluid dynamics in engineering and industrial applications.

7.References

[1] Choi SUS, Eastman JA. Enhancing thermal conductivity of fluids with nanoparticles. No. ANL/MSD/CP-84938, CONF-951135–29. (IL): Argonne National Lab, 1995.

[2] Sundar LS, Sharma KV, Singh MK, et al. Hybrid nanofluids preparation, thermal properties, heat transfer and friction factor – a review. Renew Sustain Energy Rev. 2017;68:185–198.doi:10.1016/j.rser.2016.09.108.

[3] Sarkar J, Ghosh P, Adil A. A review on hybrid nanofluids: recent research, development and applications. Renew Sustain Energy Rev. 2015;43:164–177. doi:10.1016/j.rser.2014.11.023.

[4] Devi SPA, Devi SSU. Numerical investigation of hydromagnetic hybrid Cu-Al2O3/water nanofluid flow over a permeable stretching sheet with suction. Int J Nonlin Sci Num Simul. 2016;17:249–257. doi:10.1515/ijnsns-2016-0037.

[5] Minea AA. Challenges in hybrid nanofluids behavior in turbulent flow: recent research and numerical comparison. Renew Sustain Energy Rev. 2017;71:426–434.

[6] Toghraie D, Vahid AC, Masoud A. Measurement of thermal conductivity of ZnO–TiO2/EG hybrid nanofluid. J Thermal Anal Cal. 2016;125:527–535.

[7] Hayat T, Nadeem S. Heat transfer enhancement with Ag–CuO/water hybrid nanofluid. Results Phys 2017;7:2317–2324.

[8] Jamshed W, Aziz A. A comparative entropy based analysis of Cu and Fe3O4/methanol Powell-Eyering nanofluid in solar thermal collectors subjected to thermal radiation, variable thermal conductivity and impact of different nanoparticles shape. Results Phys. 2018;9: 195–205.

[9] Ellahi R. Special issue on recent developments of nanofluids. Appl Sci. 2018;8:192.

[10] Aman S, Zokri SM, Ismail Z, et al. Effect of MHD and porosity on exact solutions and flow of a hybrid Casson-nanofluid. J Adv Res Fluid Mech Therm Sci. 2018;44:131–139.

[11] Usman M, Hamid M, Zubair T, et al. Cu-Al2O3/water hybrid nanofluid through a permeable surface in the presence of nonlinear radiation and variable thermal conductivity via LSM. Int J Heat Mass Transf. 2018;126:1347–1356.

[12] Casson N.Aflow equation for pigment oil suspensions of the printing ink type. Oxford: Pergamon Press; 1959.

[13] Ghosh S, Mukhopadhyay S. MHD slip flow and heat transfer of Casson nanofluid over an exponentially stretching permeable sheet. Int J Auto Mech Eng. 2017;14(4):4785–4804.

[14] Khan MI, Waqas M, Hayat T, et al. A comparative study of Casson fluid with homogeneousheterogeneous reactions. J Colloid Interface Sci. 2017;498:85–90. doi:10.1016/j.jcis.2017.03.024.

[15] Nayak MK, Hakeem AKA, Ganga B, et al. Entropy optimized MHD 3D nanomaterial of non- Newtonian fluid: a combined approach to good absorber of solar energy and intensification of heat transport. Comput Methods Programs Biomed. 2020;186:105131. doi:10.1016/j.cmpb.2019. 105222.

[16] Rasoola G, Chamkha AJ, Muhammad T, et al. Darcy-Forchheimer relation in Casson type MHD nanofluid flow over non-linear stretching surface. Propulsion Power Res. 2020;9(2):159–168.doi:10.1016/j.jppr.2020.04.003.

[17] Kamran A, Hussain S, Sagheer M, et al. A numerical study of magnetohydrodynamics flow in Casson nanofluid combined with Joule heating and slip boundary conditions. Results Phys.2017;7:3037–3048. doi:10.1016/j.rinp.2017.08.004.

[18] A.A. Minea, Barriers and challenges in hybrid nanofluids development and implementation, Hybrid Nanofluids Convect. Heat Transf. (2020) 255–280.

[19] M.A. Chaudhary, J.H. Merkin, A simple isothermal model for homogeneousheterogeneous reactions in boundary-layer flow. I: equal diffusivities, Fluid Dyn.Res. 16 (6) (1995) 311–333.

[20] J.H. Merkin, A model for isothermal homogeneous-heterogeneous reactions in boundary-layer flow, Math. Comput. Modelling 24 (8) (1996) 125–136.

[21] Z. He, M.B. Arain, W.A. Usman, A.R.R. Khan, T. Alzahrani, A.S. Hendy Muhammad, M.R. Ali, Theoretical exploration of heat transport in a stagnant power-law fluid flow over a stretching spinning porous disk filled with homogeneous-heterogeneous chemical reactions, Case Stud. Therm. Eng. 50 (2023) 103406.

[22] K. Gangadhar, N.R. Edukondala, K.P. Vinodh, A.J. Chamkha, Von kármán viscous pump of rotating disk in a magnetized maxwell fluid with joule heating, in:Waves Random Complex Media, 2023, pp. 1–20.

[23] K.A.M. Alharbi, S. Riasat, M. Ramzan, S. Kadry, Role of surface catalyzed reaction in the flow of temperature-dependent viscosity fluid over a rotating disk, Numer.Heat Transf. Part A Appl. (2023) 1–22.

[24] M. Sheikh, Z. Abbas, Homogeneous–heterogeneous reactions in stagnation point flow of casson fluid due to a stretching/shrinking sheet with uniform suction and slip effects, Ain Shams Eng. J. 8 (3) (2017) 467–474.

[25] M. Mustafa, T. Hayat, P. Ioan, A. Hendi, Stagnation-point flow and heat transfer of a casson fluid towards a stretching sheet, Z. Nat.forsch. A 67 (1–2) (2012)70–78.
[26] K. Bhattacharyya, Boundary layer stagnation-point flow of casson fluid and heat transfer towards a shrinking/stretching sheet, Front. Heat Mass Transf. 4 (2) (2013) 023003.
[27] S. Mukhopadhyay, P.R. De, K. Bhattacharyya, G.C. Layek, Casson fluid flow over an unsteady stretching surface, Ain Shams Eng. J. 4 (4) (2013) 933–938.
[28] W. Deebani, J. Raza, L.A. Lund, Z. Shah, M. Shutaywi, Statistical and sensitivity analysis of MHD casson nanofluid with convective boundary conditions on a stretching surface, Phys. Scr. (2024) http://dx.doi.org/10.1088/1402-4896/ada327.
[29] M. Hamid, M. Usman, Z.H. Khan, R. Ahmad, W. Wang, Dual solutions and stability analysis of flow and heat transfer of casson fluid over a stretching sheet, Phys. Lett. A 383 (20) (2019) 2400–2408.
[30] K.A. Kumar, J.V. Reddy, N. Sandeep, V. Sugunamma, Dual solutions for thermo diffusion and diffusion thermo effects on 3D MHD casson fluid flow over a stretching surface, Res. J. Pharm. Technol. 9 (8) (2016) 1187–1194.
[31] M.R. Khan, M.A. Elkotb, R.T. Matoog, N.A. Alshehri, M.A.H. Abdelmohimen, Thermal features and heat transfer enhancement of a casson fluid across a porous stretching/shrinking sheet: analysis of dual solutions, Case Stud. Therm. Eng. 28 (2021) 101594.
[32] S. Haldar, S. Mukhopadhyay, G.C. Layek, Dual solutions of casson fluid flows over a power-law stretching sheet, J. Appl. Mech. Tech. Phys. 58 (2017) 629–634.
[33] S.M. Mousavi, M.N. Rostami, M. Yousefi, S. Dinarvand, I. Pop, M.A. Sheremet, Dual solutions for casson hybrid nanofluid flow due to a stretching/shrinking sheet: a new combination of theoretical and experimental models, Chinese J. Phys. 71 (2021) 574–588.
[34] M.A. Fadhel, A. Asghar, L.A. Lund, Z. Shah, N. Vrinceanu, V. Tirth, Dual numerical solutions of casson SA–hybrid nanofluid toward a stagnation point flow over stretching/shrinking cylinder, Nanotechnol. Rev. 13 (1) (2024) 20230191.
[35] A. Sahoo, R. Nandkeolyar, Radiative heat transport of cattaneo–christov double diffusive casson nanofluid flow between two rotating disks with hall current and activation energy, Z. Angew. Math. Mech. (2023) e202200419.
[36] E. Ragupathi, D. Prakash, M. Muthtamilselvan, K. Ahn, Entropy analysis of casson nanofluid flow across a rotating porous disc with nonlinear thermal radiation and magnetic dipole, Internat. J. Modern Phys. B 37 (26) (2023) 2350308.
[37] J. Ahmed, F. Nazir, B.M. Fadhl, B.M. Makhdoum, Z. Mahmoud, A. Mohamed, I. Khan, Magneto-bioconvection flow of casson nanofluid configured by a rotating disk in the presence of gyrotactic microorganisms and joule heating, Heliyon 9 (8) (2023) e18028.
[38] M. Ramzan, S. Riasat, J.D. Chung, Y.M. Chu, M. Sheikholeslami, S. Kadry, F. Howari, Upshot of heterogeneous catalysis in a nanofluid flow over a rotating disk with slip effects and entropy optimization analysis, Sci. Rep. 11 (1) (2021) 120.